Murdock, D., Clark, I. P., & Ashfold, M. N. R. (2016). Probing Photochemically and Thermally Induced Isomerization Reactions in -Pyrone. *Journal of Physical Chemistry A*, *120*(37), 7249-7254. https://doi.org/10.1021/acs.jpca.6b06396

Probing Photochemically- and Thermally-Induced Isomerisation Reactions in α-Pyrone

Daniel Murdock,[1*] Ian P. Clark,[2] and Michael N. R. Ashfold[1*]

[1]School of Chemistry, University of Bristol, Cantock's Close, Bristol, BS8 1TS, United Kingdom

[2]Central Laser Facility, Research Complex at Harwell, Science and Technologies Facilities Council, Rutherford Appleton Laboratory, Harwell Campus, Didcot, Oxfordshire, OX11 0QX, United Kingdom

Abstract

The isomerisation dynamics of α-pyrone dissolved in CH_3CN have been probed by femtosecond 267 nm pump/ broadband infrared (IR) probe spectroscopy. A novel experimental set-up allowed the populations of the parent molecule and ring-opened photoproducts to be monitored over pump/probe time delays ranging between 2 ps and 100 μs within a single experiment, and at 5 different temperatures between 0 ºC and 40 ºC. The photochemically prepared α-pyrone(S_1) molecules decay rapidly (<10 ps) through internal conversion to the S_0 potential energy surface, with an initial quantum yield for parent molecule reformation of ~60%. Probing the antisymmetric ketene stretch region (2100-2150 cm^{-1}) confirms the presence of at least two ring-opened photoproducts, which have an *E*-configuration with respect to the central C=C double bond. These ketenes are observed to undergo two distinct, thermally driven, isomerisation processes which occur on the nanosecond and microsecond timescales, respectively. The former reaction is ascribed to thermalisation of the initially prepared *E*-isomer populations, while the slower (microsecond) process involves rotation around the central C=C double bond leading to formation of *Z*-isomers. Subsequent rapid $Z \rightarrow Z$ isomerisations (occurring on a nanosecond timescale) result in ring-closure, and a second, longer time recovery of parent molecule population. By determining rates as a function of the sample temperature, barrier heights of 0.23(3) eV and 0.43(2) eV are obtained for the $E \rightarrow E$ and $E \rightarrow Z$ transformations, respectively.

Introduction

Photoinduced ring-opening is a radiationless relaxation pathway that has been predicted and/or shown to occur in a broad range of heterocyclic molecules including furan,[1-

[4] thiophene,[5-7] α,β-unsaturated lactones,[8-14] β-glucose,[15] various substituted spiropyrans,[16-18] and DNA bases.[19] Recent work from our group has used time-resolved infrared (TRIR) spectroscopy to investigate UV-induced ring-opening of several S- and O-containing heterocycles,[20,21] and has attempted to elucidate how the potential energy landscape influences such reactions and resultant quantum yields for ring-opened products. In particular, a recent study on the dynamics of α-pyrone following femtosecond pulsed laser irradiation at 310 nm, indicated that a maximum of 32% of the initially excited molecules were reacting to form photoproducts.[21] Probing the antisymmetric ketene stretch region between 2100 cm^{-1} and 2150 cm^{-1} confirmed the presence of at least two (out of a possible eight, see figure 1) ring-opened photoproducts which were formed highly vibrationally excited on the S_0 potential energy surface (PES) and relaxed on a picosecond timescale. Following vibrational relaxation, these isomers were observed to equilibrate with a 2 ns time constant The disparity between the timescales recorded for forming these initial photoproducts and for parent molecule recovery (< 10 ps) and that seen for the ketene equilibration (~2 ns) led us to propose that the latter process was a thermally driven isomerisation taking place after radiationless transfer to the ground electronic PES.

One interesting feature highlighted in our recent study[21] was an apparent inconsistency with the results of an earlier UV pump/IR probe experiment.[14] Arnold *et al.* observed a parent molecule recovery of ~95 % over a 2.9 μs timescale[14] (*c.f.* an asymptotic 68% recovery within 100 ps observed *via* our 310 nm fs TRIR experiments). The instrument response function of this earlier experiment was such that spectra were only recorded for pump/probe time delays greater than 200 ns, compared to the longest time delay of 3 ns probed in our earlier experiments. While it is possible that the differing dynamics could be a solvent effect (Arnold *et al.* used cyclohexane, while acetonitrile was used in our experiments), we postulated that the 2.9 μs time constant could instead be evidence of a second, slower, isomerisation process occurring on the ground state PES.

Support for the hypothesis of two sequential thermally-driven isomerisation processes was provided by results obtained from complementary *ab-initio* investigations of the possible ring-open isomers of α-pyrone.[9,21] These calculations predicted eight conformers, depicted in figure 1, which can be sub-divided into four *Z*- (I, II, V, and VI) and four *E*- (III, IV, VII, VIII) isomers depending upon the orientation around the central C=C bond. Of these eight ring-open structures, isomer VI is unstable with respect to ring-closure, and thus provides a

potential route to reformation of the parent α-pyrone. $E \rightarrow E$ and $Z \rightarrow Z$ isomerisations require rotation around C–C single bonds, and are therefore likely to be relatively facile; in contrast, $E \leftrightarrow Z$ transformations are hindered by the requirement for rotation around the central C=C double bond. In our previous paper,[21] we argued that *E*-isomers are the dominant initial photoproducts in solution, and that the nanosecond timescale ketene equilibration was due to thermalisation of the nascent *E*-isomer population and that the 2.9 μs lifetime extracted by Arnold *et al.*[14] could be a measure of the $E \rightarrow Z$ isomerisation rate of ring-open photoproducts. Once formed, the *Z*-conformers should undergo further $Z \rightarrow Z$ isomerisations on a relatively rapid (nanosecond) timescale. Since one of the *Z*-conformers, VI, is unstable with respect to ring-closure, the parent α-pyrone population should therefore exhibit a second, microsecond timescale, recovery.

In this paper, we report the application of time-resolved infrared absorption spectroscopy to probe the photochemical and thermal isomerisation dynamics of α-pyrone following UV-excitation at 267 nm. A combination of optical delay lines and electronic delays[22] has allowed the response of the system to be studied for pump/probe delay times (Δt) ranging from 2 ps out to 100 μs in a single experiment – allowing direct comparison of data collected over the complete dynamical range investigated by the previous[14,21] endeavours. Further, these experiments have been performed at five temperatures between 0 ºC and 40 ºC, allowing the isomerisation barriers to be determined and compared to previous *ab-initio* predictions.[9,21]

Experimental Methodology

The TRIR data was recorded using the time-resolved multiple probe spectroscopy ($TR^{M}PS$) set-up at STFC's ULTRA facility within the Central Laser Facility.[22] This provides pump/probe time delays from <1 ps to 1 ms within a single experiment. Briefly, two titanium sapphire amplifiers with different repetition rates (1 kHz and 10 kHz) are synchronized by seeding both with the output from a single titanium sapphire oscillator (68 MHz). Full details concerning the synchronization of the lasers and acquisition of varying time-delays can be found in Ref. 22. The output from the 10 kHz amplifier generated the broadband (~500 cm^{-1} bandwidth) IR probe pulses *via* difference frequency generation in a tunable optical paramagnetic amplifier (OPA) system. The 267 nm pump radiation was produced by frequency tripling the output from the 1 kHz amplifier. The pump and probe pulses were

overlapped in the sample with their linear polarization vectors aligned at the magic angle before the transmitted IR radiation was dispersed by a grating onto a 128 element mercury cadmium telluride array detector. Temperature control (0 ºC - 40 ºC) of the α-pyrone/CH_3CN solutions was achieved through use of a thermostated water/ethylene glycol bath. α-Pyrone (90%) and CH_3CN (spectrophotometric grade) were purchased from Sigma-Aldrich and used without further purification. The sample (20 mM) was flowed continuously through a Harrick cell with a 100 μm PTFE spacer between CaF_2 windows. Sampling artifacts induced by the UV-pumped volume flowing out of the interaction region before being interrogated by the IR-probe pulse are unlikely to be significant over the pump/probe time delays used in these experiments.

Results and Discussion

Figures 2(a) and 2(b) display TRIR spectra obtained by pumping a 20 mM solution of α-pyrone/CH_3CN at 267 nm and setting the probe to cover the 1500-1775 cm^{-1} region. The solution was held at a temperature of 21 ºC (spectra recorded at different temperatures are shown in the Supporting Information (SI)), and the pump-probe time delays span the range from 2 ps out to 1 ns (figure 2(a)), and 1 ns to 100 μs (figure 2 (b)). Four negative going features (henceforth termed bleaches), reflecting the depletion of α-pyrone(S_0) population induced by the 267 nm pump pulse are present, centered around 1545, 1620, 1720 and 1735 cm^{-1}. As the pump/probe time delay increases, the magnitudes of these bleaches decrease, indicating repopulation of the parent ground state. It is clear from the 1720 cm^{-1} feature that recovery of the α-pyrone(S_0) population is occurring on at least two distinct time scales, with figure 2(a) demonstrating an initial partial recovery (~60 %) between 2 and 250 ps, and a second slower recovery occurring at pump/probe time delays greater than ~ 1 μs (figure 2(b)). In addition to the four bleach features, several positive going absorption peaks are also present. At early times ($\Delta t<50$ ps), a broad absorption covering the 1620 – 1730 cm^{-1} range is seen (this can be seen more clearly in the spectral decomposition presented in fig. S5 of the SI). This feature narrows and shifts to higher wavenumber as Δt increases, characteristic of vibrational cooling. As with the previous experiments[21] performed using 310 nm excitation, we assign this feature to vibrationally hot α-pyrone (S_0) molecules. The positive features centred around 1560, 1600, and 1660 cm^{-1} are absent at the very earliest times, before growing in with increasing Δt, and are thus attributable to photoproduct formation. Closer

analysis of the peak around 1660 cm^{-1} reveals a slight red shift in the peak centre occurring on the nanosecond timescale (figure 2(b)). The time for this spectral shift is too slow for it to be explained by vibrational cooling of photoproducts, suggesting that it is due to isomerisation between the ring opened *E*-isomers instead. These carbonyl product features are then seen to decay over longer times, disappearing completely by ~10 μs.

The build-up and eventual decay of photoproducts can be more clearly observed by changing the probe region to cover the antisymmetric ketene-stretching region between 1970 - 2170 cm^{-1}, which allows direct observation of the ring-opened ground state species. At early pump/probe time delays (figure 3(a)), an extremely broad (FWHM ≈ 75 cm^{-1}) transient absorption centered around 2075 cm^{-1} is observed, which narrows and blue shifts on a picosecond timescale. After the initial vibrational cooling is complete (Δt ≈ 40 ps), two peaks centered around 2115 cm^{-1} and 2125 cm^{-1} are clearly discernable. As before,[21] we assign these features as the signatures of at least two ring-open photoproducts with *E*-configurations. Isomerisation between the photochemically prepared *E*-isomers then occurs on a nanosecond timescale, as manifest by the 2115 cm^{-1} peak decreasing in intensity, accompanied by a concomitant growth of the 2125 cm^{-1} feature. This isomerisation is seen to continue at later times (Δt > 1 ns; figure 3(b)), until a single ring-opened photoproduct dominates the observed spectra. After a pump/probe time delay of ~100 ns the population of this final ring-opened species begins to decay, and has disappeared completely by ~10 μs.

Kinetic Analysis

The TRIR spectra of α-pyrone were analysed by decomposing each time slice in terms of model basis functions. Further details and representative decompositions are given in the SI. Figure 4(a) depicts the time dependent population of α-pyrone (S_0; ν=0) obtained following 267 nm irradiation of a solution held at 21 ºC. The bleach signal remains constant for ~10 ps before undergoing a partial (60%) recovery which is essentially complete by Δt = 100 ps. This sigmoidal bleach recovery can be interpreted as the time required for the photoexcited α-pyrone(S_1) molecules to undergo internal conversion to high lying regions of the S_0 electronic manifold, followed by vibrational relaxation and eventual reformation of α-pyrone(S_0; ν=0). After ~250 ns, a secondary bleach recovery becomes apparent. As with the initial parent molecule repopulation, this secondary recovery is also incomplete. In total, ~5 -

10% of the photoexcited α-pyrone molecules do not recover – indicating that there are some long-lived photoproducts. The observation of a dual bleach recovery, along with the respective time constants, reconciles the differing observations reported in our previous paper[21] (~68 % parent molecule reformation within 250 ps) with those reported in the earlier study of Arnold *et al*.[14] (95% bleach recovery determined by probing over pump/probe time delays spanning 200 ns < Δt < 25 μs).

The kinetics of the photoproduct peaks located at 1560, 1600, and 1660 cm^{-1} are also shown in figure 4(a). The three vibrational bands are treated using a single "product" basis spectrum, and consequently a single kinetic trace describes the time dependent behaviour for all features. Because the product carbonyl features are fit using a single basis function, any isomerisation between ring-opened forms is not modeled; instead, this trace acts as a measure of the total photoproduct population. Such an approach implies that the relative intensities of these three carbonyl peaks are insensitive to isomerization – an assumption that the experimental data tends to support. The experimentally observed growth of the product carbonyl bands is rapid ($\tau_{rise} \approx 10$ ps), and is thus a convolution of the photolytic ring opening and vibrational cooling rates of the nascent photoproducts. Once formed, the population of ring-opened photoproducts is seen to persist for several hundred nanoseconds, before eventually decaying to zero after ~10 μs. This complete decay is in contrast with the ~90% recovery demonstrated by the α-pyrone(S_0; ν=0) population and indicates that a small fraction (<10%) of the initially photoexcited molecules react to form a different, unobserved, product species. Previous work on the UV-induced photochemistry of α-pyrone as a matrix isolated species[9] or in solution[14,23] suggests that this missing fraction is likely a bicyclic Dewar isomer.

The time-dependent populations of the ring-opened *E*-isomers can be monitored through their antisymmetric ketene features located at 2115 cm^{-1} and 2125 cm^{-1}. At early times (Δt < 40 ps), the degree of vibrational excitation of the photoproducts is such that a single broad band is observed, preventing any isomer specific information being obtained. After this time, the two ketene peaks are resolvable, and their integrated areas are depicted in figure 4(b). The ketene data highlights at least two different isomerisations occurring on very different timescales. The first of these is a thermalisation of the *E*-isomer populations occurring within the first 10 ns (shown by a decay in the 2115 cm^{-1} peak and concomitant increase in the area of the 2125 cm^{-1} feature), and the second – occurring at a far slower rate

– results in the decay of all ring-opened species. This latter reaction is the result of sequential $E \rightarrow Z$ and $Z \rightarrow Z$ isomerisations which result in the eventual reformation of the ring-closed parent molecule.

The time-dependent populations of α-pyrone and its ring-opened photoproducts shown in figures 4(a) and 4(b) encourages fitting of the data according to the following simplified kinetic scheme (ketene 1 is the photoproduct associated with the 2115 cm^{-1} peak, and ketene 2 gives rise to the 2125 cm^{-1} feature):

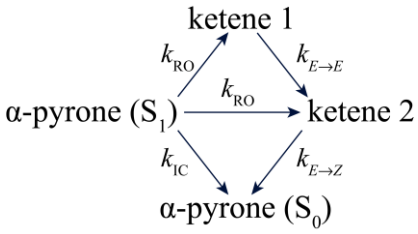

where k_{RO} and k_{IC} are the ring-opening and $S_1 \rightarrow S_0$ internal conversion rates, $k_{E\rightarrow E}$ is the $E \rightarrow E$ isomerisation rate, and $k_{E\rightarrow Z}$ is an effective rate coefficient describing the sequential $E \rightarrow Z$ and $Z \rightarrow Z$ isomerisations necessary for ring-closure and subsequent reformation of the α-pyrone parent molecule. Analytical solutions for the time-dependent populations of interest were obtained[24] (with the photoproduct carbonyl intensity of figure 4(a) being described by the sum of ketene 1 and ketene 2), and the solid lines depicted in figures 4(a) and 3(b) show the fits to the experimental data. The short lifetime of the photoprepared α-pyrone(S_1) state (<10 ps) means that the experimentally determined ring opening and internal conversion rates are heavily convoluted with vibrational lifetimes (*vide supra*), and are ill-described by the kinetic scheme. Therefore, the values of k_{RO} and k_{IC} were fixed at 0.2 and 0.6 ns^{-1}, respectively (ensuring a quantum yield of 0.6 for internal conversion), and only pump/probe time delays of $\Delta t \geq 40$ ps were included in the fit.

Figure 5 shows the time dependent populations of the 2125 cm^{-1} ketene feature recorded at 0 ºC, 13 ºC, and 40 ºC. As expected for a thermally controlled process, an increase in temperature sees a concurrent increase in both the $E \rightarrow E$ and $E \rightarrow Z$ isomerisation rates. The solid lines are fits to the data using the kinetic scheme, with the best-fit values extracted for $k_{E\rightarrow E}$ and $k_{E\rightarrow Z}$ shown (along with those obtained at 7 ºC and 21 ºC) in Table 1. Arrhenius plots of the variation of $k_{E\rightarrow E}$ and $k_{E\rightarrow Z}$ with temperature are shown in figures 6(a) and 5(b), along with the corresponding best-fit lines linking the data points. The Arrhenius

plots indicate barrier heights of 0.23(3) eV and 0.43(2) eV for the $E \rightarrow E$ and $E \rightarrow Z$ transformations, respectively. These values can be compared to the calculated ground state potential barriers obtained for the interconversion pathways involving rotation around one bond (where rotations around C–C single bonds allow for $E \rightarrow E$ or $Z \rightarrow Z$ isomerisation, while an $E \rightarrow Z$ configurational change requires rotation about the central C=C bond) presented previously.[9,21] Calculations of the optimised transition state structures at the MP2/cc-pVTZ/CH_3CN PCM level of theory[21] predicted barriers of ~0.4 eV for C–C single bond rotations, in reasonable agreement with the value obtained experimentally. The calculated $E \rightarrow Z$ barriers (>2 eV), in contrast, are far higher than the 0.43 eV value returned by the present studies. The poor agreement between experimental and calculated reaction barriers for the $E \rightarrow Z$ isomerisation are consistent with recent work by Maeda *et al.*,[25] who highlighted how the true minimum energy pathways linking conformational isomers can be extremely complicated and involve numerous transition states. These results suggest that an isolated rotation around the central C=C bond is a drastic oversimplification of the true isomerisation pathway.

Summary and Conclusions

The photochemically and thermally driven isomerisation dynamics of α-pyrone in CH_3CN solution have been probed over times ranging from 2 ps out to 100 μs. Following irradiation at 267 nm, α-pyrone(S_1) decays rapidly (estimated lifetime <10 ps). Internal conversion leads to reformation of the parent molecule with a quantum yield of ~60%, while probing the antisymmetric ketene stretch region confirms the presence of ring-opened photoproducts. Following vibrational cooling, the initially formed *E*-isomers thermalise on a 1-5 ns timescale, as gauged by the evolving intensities of two closely spaced ketene absorption features. A later, secondary, isomerisation is observed occurring on a microsecond timescale which consumes all the ring-open photoproduct population. The concomitant bleach recovery indicates that these photoproducts are ring closing, leading to reformation of the parent molecule. The parent bleach signal does not fully recover, however; the residual (<10%) of photoexcited molecules are assumed to react to form an alternative (unobserved) product, most probably a bicyclic Dewar isomer. We assign the slower isomerisation process to sequential $E \rightarrow Z$ and $Z \rightarrow Z$ transformations which allow for formation of the unstable

isomer VI and thence ring-closure. By varying the temperature of the reaction cell, barrier heights of 0.23 eV and 0.43 eV for the $E \rightarrow E$ and $E \rightarrow Z$ isomerisations, respectively, have been obtained, and compared to previous *ab-initio* estimations. While the $E \rightarrow E$ isomerisation can be described reasonably by considering rotations around single C–C bonds, the value obtained for the $E \rightarrow Z$ transformations hints at the underlying complexity of the true minimum energy pathway for this reaction.

Author Information

Corresponding authors

D.M. (e-mail: daniel.murdock@bristol.ac.uk)

M.N.R.A. (e-mail: mike.ashfold@bristol.ac.uk. telephone: +44 117 9288312)

Notes

The authors declare no competing financial interest

Acknowledgements

This work was supported by the European Research Council through ERC Advanced Grant 290966 CAPRI and STFC via access to the ULTRA laser within the Central Laser Facility. The authors thank Rebecca A. Ingle and Dr. Thomas A. A. Oliver for their assistance in collecting the experimental data presented in this paper.

Supporting Information

Time-resolved infrared absorption spectra of α-pyrone/CH_3CN recorded at 0 ºC, 7 ºC, 13 ºC, and 40 ºC. Details and example fits from the decomposition procedures used in the extraction of kinetic traces. Kinetic fits of data recorded at 0 ºC, 7 ºC, 13 ºC, and 40 ºC

References

(1) Stenrup, M.; Larson, Å. A Computational Study of Radiationless Deactivation Mechanisms of Furan. *Chem. Phys.* **2011**, *379*, 6–12.

(2) Gromov, E. V.; Léveque, C.; Gatti, F.; Burghardt, I.; Köppel, H. Ab Initio Quantum Dynamical Study of Photoinduced Ring Opening in Furan. *J. Chem. Phys.* **2011**, *135*, 164305.

(3) Gromov, E. V.; Trofimov, A. B.; Gatti, F.; Köppel, H. Theoretical Study of Photoinduced Ring-Opening in Furan. *J. Chem. Phys.* **2010**, *133*, 164309.

(4) Gavrilov, N.; Salzmann, S.; Marian, C. M. Deactivation via Ring Opening: a Quantum Chemical Study of the Excited States of Furan and Comparison to Thiophene. *Chem. Phys.* **2008**, *349*, 269–277.

(5) Stenrup, M. Theoretical Study of the Radiationless Deactivation Mechanisms of Photo-Excited Thiophene. *Chem. Phys.* **2012**, *397*, 18–25.

(6) Cui, G.; Fang, W. Ab Initio Trajectory Surface-Hopping Study on Ultrafast Deactivation Process of Thiophene. *J. Phys. Chem. A* **2011**, *115*, 11544–11550.

(7) Salzmann, S.; Kleinschmidt, M.; Tatchen, J.; Weinkauf, R.; Marian, C. M. Excited States of Thiophene: Ring Opening as Deactivation Mechanism. *Phys. Chem. Chem. Phys.* **2008**, *10*, 380–392.

(8) Kuş, N.; Breda, S.; Reva, I.; Tasal, E.; Ogretir, C.; Fausto, R. FTIR Spectroscopic and Theoretical Study of the Photochemistry of Matrix-Isolated Coumarin. *Photochem. Photobiol.* **2007**, *83*, 1237–1253.

(9) Breda, S.; Reva, I.; Lapinski, L.; Fausto, R. Matrix Isolation FTIR and Theoretical Study of α-Pyrone Photochemistry. *Phys. Chem. Chem. Phys.* **2004**, *6*, 929–937.

(10) Breda, S.; Reva, I.; Fausto, R. UV-Induced Unimolecular Photochemistry of 2(5H)-Furanone and 2(5H)-Thiophenone Isolated in Low Temperature Inert Matrices. *Vib. Spectrosc.* **2009**, *50*, 57–67.

(11) Fausto, R.; Breda, S.; Kuş, N. Photochemistry of Six- and Five-Membered-Ring α,β-Unsaturated Lactones in Cryogenic Matrices. *J. Phys. Org. Chem.* **2008**, *21*, 644–651.

(12) Krauter, C. M.; Möhring, J.; Buckup, T.; Pernpointner, M.; Motzkus, M. Ultrafast Branching in the Excited State of Coumarin and Umbelliferone. *Phys. Chem. Chem. Phys.* **2013**, *15*, 17846–17861.

(13) Tatchen, J.; Marian, C. M. Vibronic Absorption, Fluorescence, and Phosphorescence Spectra of Psoralen: a Quantum Chemical Investigation. *Phys. Chem. Chem. Phys.* **2006**, *8*, 2133–2144.

(14) Arnold, B. R.; Brown, C. E.; Lusztyk, J. Solution Photochemistry of 2H-Pyran-2-one: Laser Flash Photolysis with Infrared Detection of Transients. *J. Am. Chem. Soc.* **1993**, *115*, 1576–1577.

(15) Tuna, D.; Sobolewski, A. L.; Domcke, W. Electronically Excited States and Photochemical Reaction Mechanisms of B-Glucose. *Phys. Chem. Chem. Phys.* **2014**, *16*, 38–47.

(16) Rini, M.; Holm, A.-K.; Nibbering, E. T. J.; Fidder, H. Ultrafast UV-Mid-IR Investigation of the Ring Opening Reaction of a Photochromic Spiropyran. *J. Am.*

Chem. Soc. **2003**, *125*, 3028–3034.

(17) Liu, F.; Morokuma, K. Multiple Pathways for the Primary Step of the Spiropyran Photochromic Reaction: a CASPT2//CASSCF Study. *J. Am. Chem. Soc.* **2013**, *135*, 10693–10702.

(18) Prager, S.; Burghardt, I.; Dreuw, A. Ultrafast C_{Spiro}–O Dissociation via a Conical Intersection Drives Spiropyran to Merocyanine Photoswitching. *J. Phys. Chem. A* **2014**, *118*, 1339–1349.

(19) Perun, S.; Sobolewski, A. L.; Domcke, W. Photostability of 9H-Adenine: Mechanisms of the Radiationless Deactivation of the Lowest Excited Singlet States. *Chem. Phys.* **2005**, *313*, 107–112.

(20) Murdock, D.; Harris, S. J.; Luke, J.; Grubb, M. P.; Orr-Ewing, A. J.; Ashfold, M. N. R. Transient UV Pump-IR Probe Investigation of Heterocyclic Ring-Opening Dynamics in the Solution Phase: the Role Played by nσ* States in the Photoinduced Reactions of Thiophenone and Furanone. *Phys. Chem. Chem. Phys.* **2014**, *16*, 21271–21279.

(21) Murdock, D.; Ingle, R. A.; Sazanovich, I. V.; Clark, I. P.; Harabuchi, Y.; Taketsugu, T.; Maeda, S.; Orr-Ewing, A. J.; Ashfold, M. N. R. Contrasting Ring-Opening Propensities in UV-Excited α-Pyrone and Coumarin. *Phys. Chem. Chem. Phys.* **2016**, *18*, 2629–2638.

(22) Greetham, G. M.; Sole, D.; Clark, I. P.; Parker, A. W.; Pollard, M. R.; Towrie, M. Time-Resolved Multiple Probe Spectroscopy. *Rev. Sci. Instrum.* **2012**, *83*, 103107.

(23) Corey, E. J.; Streith, J. Internal Photoaddition Reactions of 2-Pyrone and N-Methyl-2-pyridone: a New Synthetic Approach to Cyclobutadiene. *J. Am. Chem. Soc.* **1964**, *86*, 950–951.

(24) Berberan-Santos, M. N.; Martinho, J. M. G. The Integration of Kinetic Rate Equations by Matrix Methods. *J. Chem. Educ.* **1990**, *67*, 375–379.

(25) Maeda, S.; Harabuchi, Y.; Ono, Y.; Taketsugu, T.; Morokuma, K. Intrinsic Reaction Coordinate: Calculation, Bifurcation, and Automated Search. *Int. J. Quantum Chem.* **2015**, *115*, 258–269.

Table 1: Rate coefficients, time constants and their one-standard deviation uncertainties determined for the $E \rightarrow E$ and $E \rightarrow Z$ isomerisation reactions of the ring-opened photoproducts of α-pyrone at five different sample temperatures in the range 0-40 ºC.

Temperature/ºC	$k_{E \rightarrow E}$ / ns^{-1}	$\tau_{E \rightarrow E}$ /ns	$k_{E \rightarrow Z}$ / μs^{-1}	$\tau_{E \rightarrow Z}$ / μs
0	0.23(1)	4.3(2)	0.147(5)	6.8(2)
7	0.34(1)	2.94(9)	0.249(8)	4.0(1)
13	0.44(2)	2.3(1)	0.42(2)	2.4(1)
21	0.56(2)	1.79(6)	0.55(2)	1.82(7)
40	0.84(4)	1.19(6)	1.56(7)	0.64(3)

Figure Captions

Figure 1: α-pyrone and its eight ring opened isomers. The middle row depicts the four isomers having *E*-configuration with respect to the central C=C double bond, and the bottom row shows the *Z*-isomers. The numbering scheme used is the same as that presented in the work by Breda *et al.* in reference 9.

Figure 2: Time-resolved infrared absorption spectra of a 20 mM solution of α-pyrone in CH_3CN following irradiation at 267 nm and probing in the 1500 - 1775 cm^{-1} range. Panel (a) shows the spectra recorded for pump/probe time delays between 2 ps and 1 ns, and (b) between 1 ns - 100 μs. The sample cell was maintained at a temperature of 21 ºC for the duration of these measurements.

Figure 3: Time-resolved infrared absorption spectra of a 20 mM solution of α-pyrone in CH_3CN following irradiation at 267 nm and probing (a) the 1970 - 2170 cm^{-1} range, and (b) the 2090 - 2150 cm^{-1} range. Panel (a) depicts the spectra recorded for pump/probe time delays between 2 ps and 1 ns, and (b) between 1 ns - 100 μs. The sample cell was maintained at a temperature of 21 ºC for the duration of these measurements.

Figure 4: Time dependent populations of (a) α-pyrone (S_0; ν=0) and carbonyl containing photoproducts, and (b) the ketene peaks centred around 2115 cm^{-1} and 2125 cm^{-1} obtained following 267 nm irradiation and at a temperature of 21 ºC. The kinetic traces (open circles) were obtained from the spectral decomposition procedures described in the SI, and the solid lines are fits to the kinetic scheme described in the main text.

Figure 5: Normalised peak intensities of the 2125 cm^{-1} ketene feature obtained from experiments performed at 0 ºC, 13 ºC, and 40 ºC. The kinetic traces (open circles) were obtained from the spectral decomposition procedures described in the SI, and the solid lines are fits to the kinetic scheme described in the main text.

Figure 6: Arrhenius plots showing the variation of (a) $k_{E\rightarrow E}$ and (b) $k_{E\rightarrow Z}$ with temperature. The solid line is the best fit to the data, and the extracted activation energies (E_a) and pre-

exponential factors (*A*) are given in the plots.

Figure 1

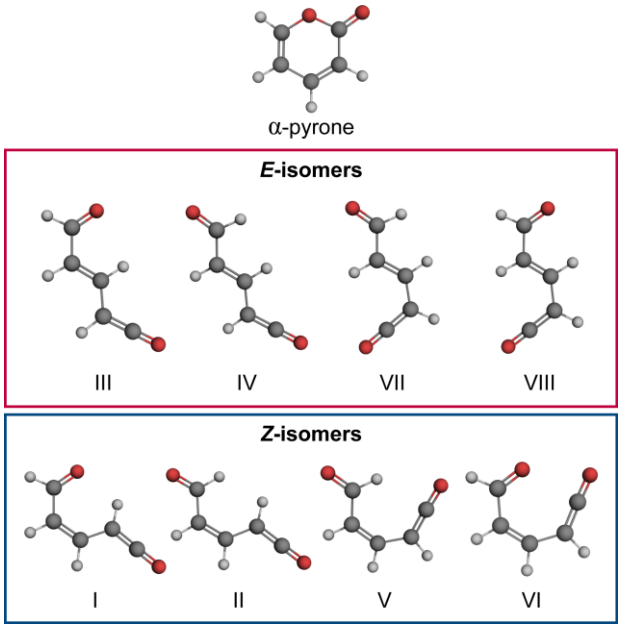

Figure 2

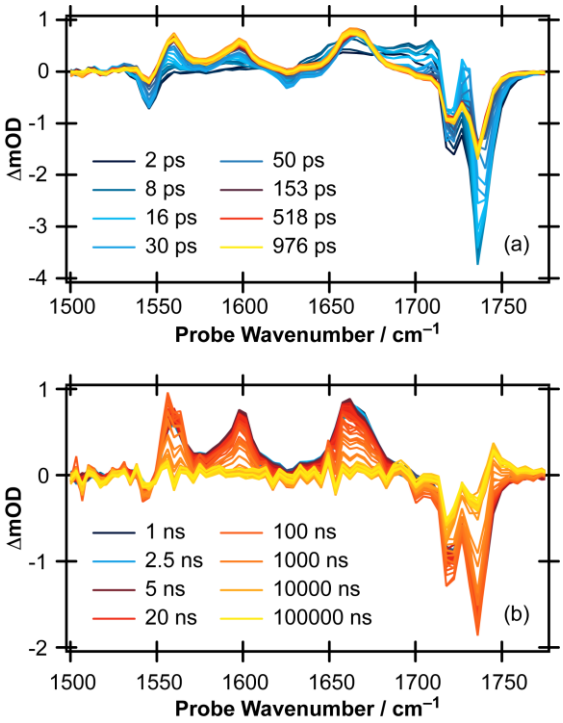
1
0
-1
-2
-3
-4
ΔmOD
2 ps
8 ps
16 ps
30 ps
50 ps
153 ps
518 ps
976 ps
(a)
1500
1550
1600
1650
1700
1750
Probe Wavenumber / cm−1
1
0
-1
-2
ΔmOD
1 ns
2.5 ns
5 ns
20 ns
100 ns
1000 ns
10000 ns
100000 ns
(b)
1500
1550
1600
1650
1700
1750
Probe Wavenumber / cm−1

Figure 3

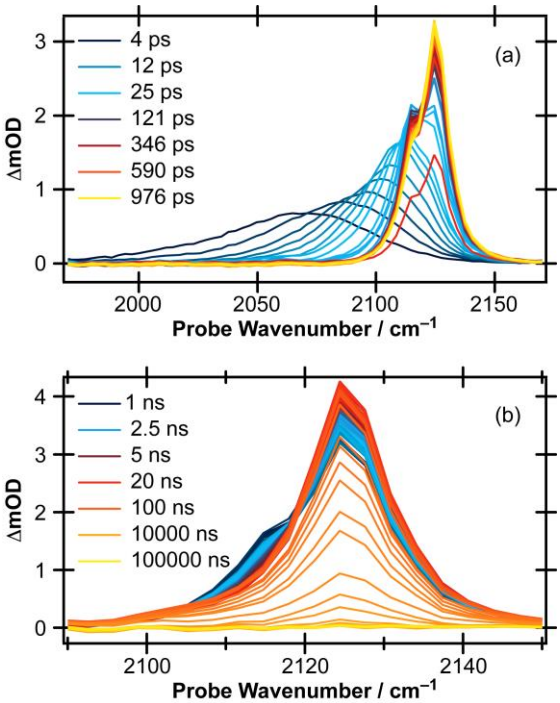
4 ps
12 ps
25 ps
121 ps
346 ps
590 ps
976 ps
(a)
ΔmOD
Probe Wavenumber / cm⁻¹
1 ns
2.5 ns
5 ns
20 ns
100 ns
10000 ns
100000 ns
(b)
ΔmOD
Probe Wavenumber / cm⁻¹

Figure 4

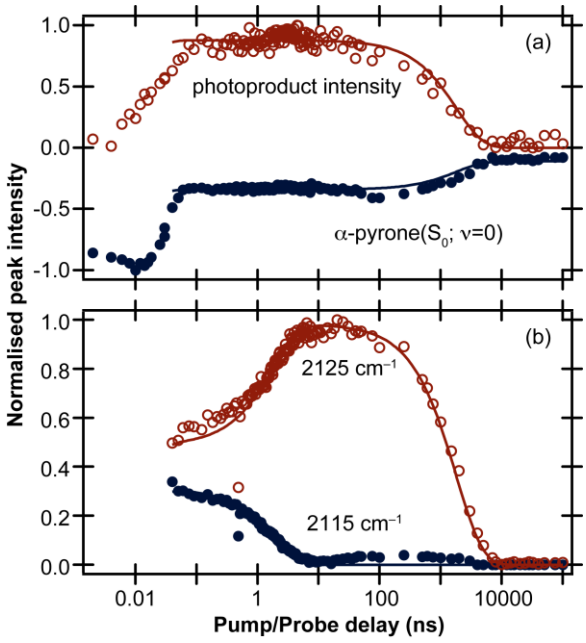
(a)
photoproduct intensity
α-pyrone(S0; ν=0)
(b)
2125 cm−1
2115 cm−1
Normalised peak intensity
Pump/Probe delay (ns)
1.0
0.5
0.0
-0.5
-1.0
0.8
0.6
0.4
0.2
0.01
1
100
10000

Figure 5

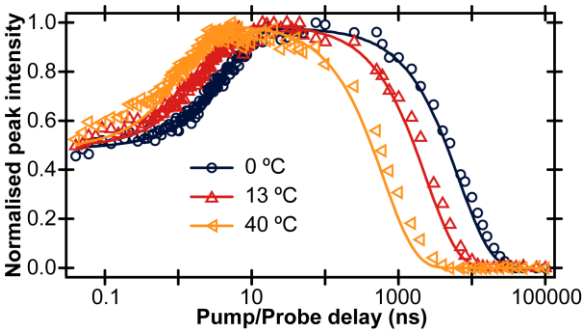
Normalised peak intensity
1.0
0.8
0.6
0.4
0.2
0.0
0.1
10
1000
100000
Pump/Probe delay (ns)
0 ºC
13 ºC
40 ºC

Figure 6

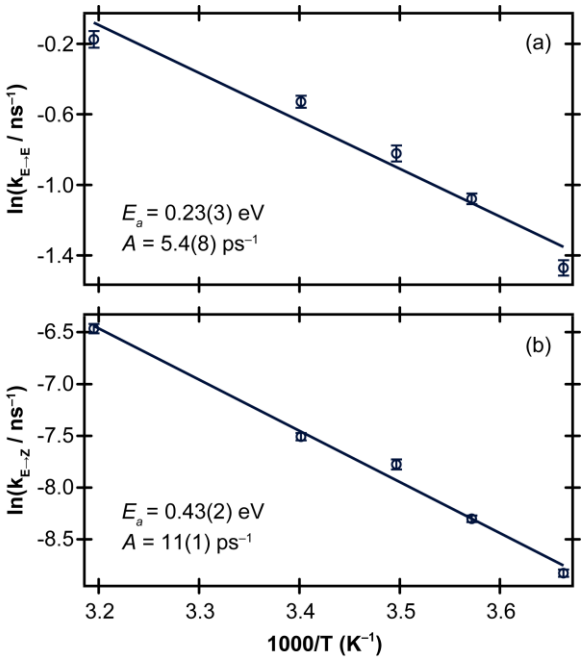
(a)
E_a = 0.23(3) eV
A = 5.4(8) ps^{-1}
$\ln(k_{E\to E}$ / ns$^{-1})$
-0.2
-0.6
-1.0
-1.4
(b)
E_a = 0.43(2) eV
A = 11(1) ps^{-1}
$\ln(k_{E\to Z}$ / ns$^{-1})$
-6.5
-7.0
-7.5
-8.0
-8.5
3.2
3.3
3.4
3.5
3.6
1000/T (K^{-1})

Table of Contents Graphic